



HAL
open science

Microstructural-based Analysis and Modelling of the Fatigue Behaviour of Cast Al-Si Alloys

Viet Duc Le, Franck Morel, Daniel Bellett, Etienne Pessard, Nicolas Saintier,
Pierre Osmond

► **To cite this version:**

Viet Duc Le, Franck Morel, Daniel Bellett, Etienne Pessard, Nicolas Saintier, et al.. Microstructural-based Analysis and Modelling of the Fatigue Behaviour of Cast Al-Si Alloys. 6th International Fatigue Design Conference, Nov 2015, Senlis, France. pp.562-575, 10.1016/j.proeng.2015.12.630 . hal-02486657

HAL Id: hal-02486657

<https://hal.science/hal-02486657>

Submitted on 21 Feb 2020

HAL is a multi-disciplinary open access archive for the deposit and dissemination of scientific research documents, whether they are published or not. The documents may come from teaching and research institutions in France or abroad, or from public or private research centers.

L'archive ouverte pluridisciplinaire **HAL**, est destinée au dépôt et à la diffusion de documents scientifiques de niveau recherche, publiés ou non, émanant des établissements d'enseignement et de recherche français ou étrangers, des laboratoires publics ou privés.

6th Fatigue Design conference, Fatigue Design 2015

Microstructural-based analysis and modelling of the fatigue behaviour of cast Al-Si alloys

Viet-Duc LE^{a,b,c,*}, Franck MOREL^a, Daniel BELLETT^a, Etienne Pessard^a,
Nicolas SAINTIER^b, Pierre OSMOND^c

^aArts et Métiers ParisTech, CER Angers - Laboratoire LAMPA - 2 Bd du Ronceray, 49035 Angers Cedex 1, FRANCE

^bArts et Métiers ParisTech, CER Bordeaux - Laboratoire I2M - Esplanade des Arts et Métiers, 33405 TALENCE Cedex, FRANCE

^cPSA Peugeot Citroën, 18 rue des fauvelles, 92256 La Garenne-Colombes cedex, FRANCE

Abstract

This paper describes a microstructural-based high cycle fatigue behaviour model applied to cast Al-Si alloys used in an automobile context. These materials are characterized by the presence of different microstructural heterogeneities at different scales: the aluminium matrix (DAS/SDAS and the precipitation hardening level), inclusions (Si particles and intermetallic) and casting defects (porosity). It is shown that the effects of these factors on the HCF damage mechanisms are important and can depend on the loading mode. A multiaxial fatigue test campaign has been carried out using three cast aluminium alloys, fabricated by different casting processes (gravity die casting and lost foam casting), associated with several heat treatments (T7 and Hot Isostatic Pressing-HIP). The HIP treatment is used to eliminate or minimise the porosity. The first part of the article is dedicated to the experimental characterization of the HCF damage mechanisms. With regard to the effect of the casting defects, a study of natural fatigue crack growth and artificial long crack growth is presented and subsequently used to choose an appropriate fatigue strength criterion to take into account the effect of defects, for different loading modes (tension, torsion and combined tension-torsion). Finally, a flexible modelling framework, providing the possibility of combining any two suitable criteria, which leads to the construction of a multiaxial Kitagawa-Takahashi diagram, is used.

Keywords: High cycle fatigue; multiaxial; cast aluminium alloy; defect; modelling; probabilistic;

1. Introduction

Cast aluminium alloys have been used in automobile components for many years because of their low density and excellent thermal conductivity. These components are subjected to cyclic mechanical loads which can cause the fatigue crack initiation, as well as functional failure of the structure. It has been demonstrated [1–6] that in the high cycle fatigue domain, one of the principal parameters controlling the

Email address: viet-duc.le@ensam.eu (Viet-Duc LE)

fatigue strength of cast Al-Si alloys is the presence of different microstructural heterogeneities which occur in the form of inclusions (Si particles, inter-metallic), casting defects (micro-shrinkage or degassing pores) and the aluminium matrix (often characterized by the DAS and/or SDAS and the precipitation hardening level). These characteristics depend principally on casting process (gravity die cast, lost foam cast, sand cast..) as well as the post-heat treatment (T6/T7, hot isostatic pressing (HIP)).

The principal aim of this work is to decouple the roles of these different heterogeneities on the creation of fatigue damage and the resulting fatigue strength of cast aluminium alloys. In order to achieve this aim, an extensive multi-axial HCF test campaign was conducted, including pure tension, pure torsion, combined tension-torsion and equibiaxial tension, on three different Al-Si alloys: gravity die cast - T7 heat treated (alloy A), lost foam cast-T7 heat treated (alloy B) and lost foam cast-HIP-T7 heat treated (alloy C). Thanks to these different processes, three very different microstructures and casting defect populations have been obtained in order to distinguish the roles of the different microstructural heterogeneities.

In the first part of this paper, the characterisation of different fatigue crack initiation mechanisms highlighting the role of the heterogeneities, will be presented. Based on these empirically observed mechanisms, a flexible modelling framework (initiated by Pessard et al. [7] and Koutiri et al. [8]), is used to study cast aluminium alloys.

2. Material and experimental conditions

Fig.1 shows typical microstructural images of the aluminium alloys under investigation which highlight the different microstructural heterogeneities that can be found (i.e. silicon particles in the eutectic zones, inter-metallic inclusions, micro-shrinkage/degassing pores and the dendrite size defined by the DAS and SDAS).

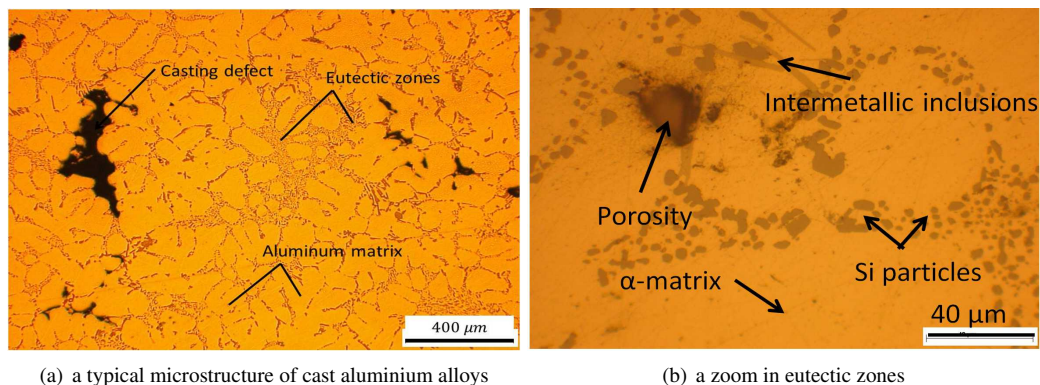


Fig. 1. Micro-structural heterogeneities of cast aluminium alloys

2.1. Material preparation and microstructure

The three cast aluminium alloys investigated in this study are referred to as alloys A, B and C. Table 1 lists the chemical compositions, casting processes and heat treatments for each studied material. It is important to note that because the mould used to cast the Alloy B was in the form of a sheet, its microstructure and defect size distribution are not representative of the real material present in industrially cast cylinder heads. The microstructures of the three materials are shown in figure 2.

The aluminium matrix is typically characterized by the Dendrite Arm Spacing (DAS) and/or Secondary Dendrite Arm Spacing (SDAS). These quantities can be determined by identifying individual aluminium dendrites. The SDAS or the distance between the secondary dendrite arms is then measured (see Fig.3). Forty dendrites in each material were measured. In addition, the α phase matrix of the material can be characterised by its micro-hardness which is controlled principally by precipitation hardening. Tab.2 summarizes the SDAS and the micro-hardness measurement of the aluminium matrix of the three alloys.

Alloy	Chemical Composition (wt.)	Forming process	Heat Treatment
A	7%Si, 0.3%Mg, 0.5%Cu, Remainder Al	Gravity Die Cast	T7
B	7%Si, 0.3%Mg, Remainder Al	Lost Foam Cast	T7
C	7%Si, 0.3%Mg, Remainder Al	Lost Foam Cast	HIP+T7

Table 1. Chemical compositions, casting processes and heat treatments of three studied material

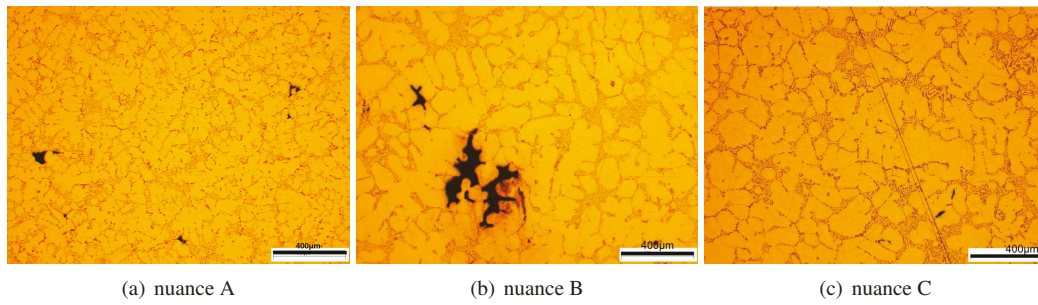


Fig. 2. Microstructures of three studied alloys

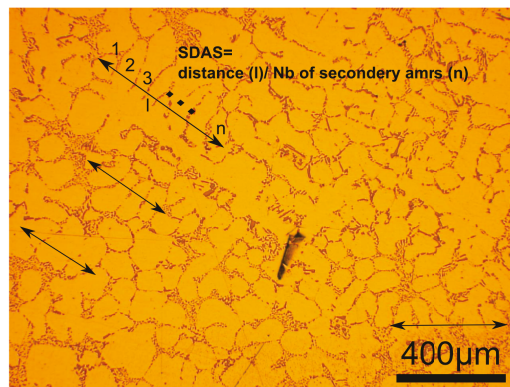


Fig. 3. SDAS measurement method

Alloy	SDAS ($\mu \pm s$)(μm)	Micro-hardness ($\mu \pm s$)(Hv0.025)
A	42.3 \pm 9.7	113.8 \pm 2.8
B	77.3 \pm 18.9	99 \pm 9
C	91.4 \pm 32.8	92 \pm 13

Table 2. DAS/SDAS and micro-hardness of aluminium matrix of three studied alloys

In order to characterise the size distribution of the casting defects (degassing and/or micro-shrinkage pores) in these materials, the metallography methodology proposed by Murakami [9] has been employed. When using this methodology, the defect size distribution is determined from optical microscopic observations of polished samples. In particular, the maximum defect size in each standard inspection area of size S_0 , is measured. The resulting distribution corresponds to the extreme value distribution related to the area S_0 . From this point of view, the maximum defect size in a given surface (or volume) can be extrapolated using the Gumbel distribution [9]. The defect size distributions determined for the three alloys are shown in figure 4. The maximum defect sizes observed on the polished surfaces of alloys A, B and C are approximately $300\mu\text{m}$, $500\mu\text{m}$ and $50\mu\text{m}$ respectively. Furthermore, it can be seen that the Gumbel distribution results in good approximations for the three alloys.

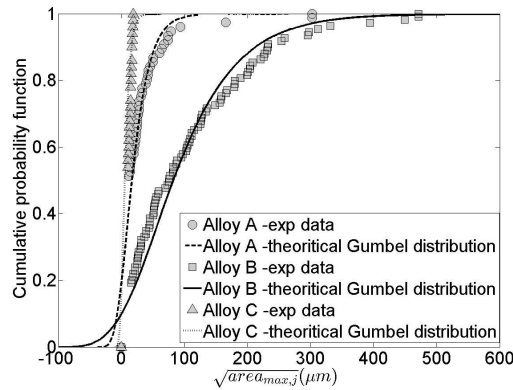


Fig. 4. Defect size distributions of the three alloys characterized by microscopic observations

2.2. Experimental conditions: fatigue tests

All of the fatigue tests presented below were carried out at ambient temperature and pressure in laboratory air. In order to be able to ignore the volume effect, all fatigue tests were conducted with the same specimen geometry (except for the fatigue tests under plane bending loads of alloy A, reported in the work of Koutiri et al.[10]), as shown in figure 5.

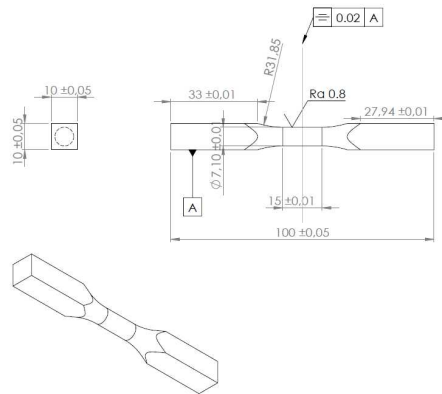


Fig. 5. Specimen for tension, torsion and combined tension-torsion fatigue tests

The fatigue tests were conducted in load control using a sinusoidal waveform, with a load ratio of $R=-1$. The pure tension tests were conducted on a Rumul Testronic resonant testing machine at 90-110 Hz while the pure torsion tests were conducted on a Rumul Cractronic resonant testing machine at 70-90Hz. The in-phase combined tension-torsion tests with a biaxiality ratio of $k = \tau_a/\sigma_a = 0.5$ were performed on a Bose electromagnetic testing machine at 20-30 Hz. The fatigue tests were conducted using the staircase technique, at a maximum life of $2 \cdot 10^6$ cycles. The stopping criteria were chosen to ensure the presence of a fatigue crack of approximately 3 mm in length.

3. High cycle fatigue crack initiation mechanisms of cast aluminium alloys

Fig.6 and 7 summarises the crack initiation mechanisms observed on the surface of the three alloys for the different loading modes, (using an optical microscope) as well as on the fatigue failure surfaces (using a scanning Electron Microscope SEM).

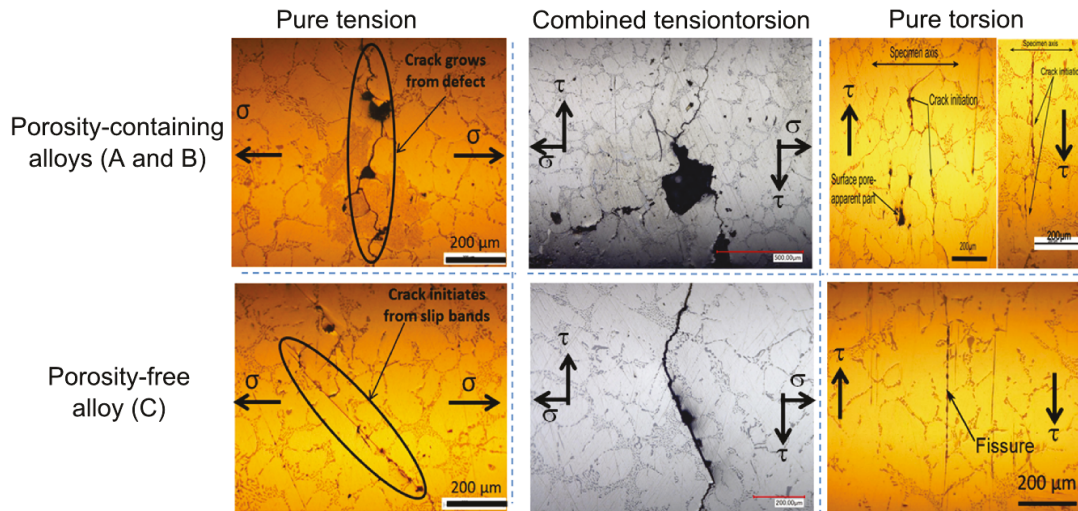


Fig. 6. Fatigue damage mechanisms of alloys A, B and C for three loading modes (pure tension, combined tension-torsion and pure torsion), observed on the specimen surfaces

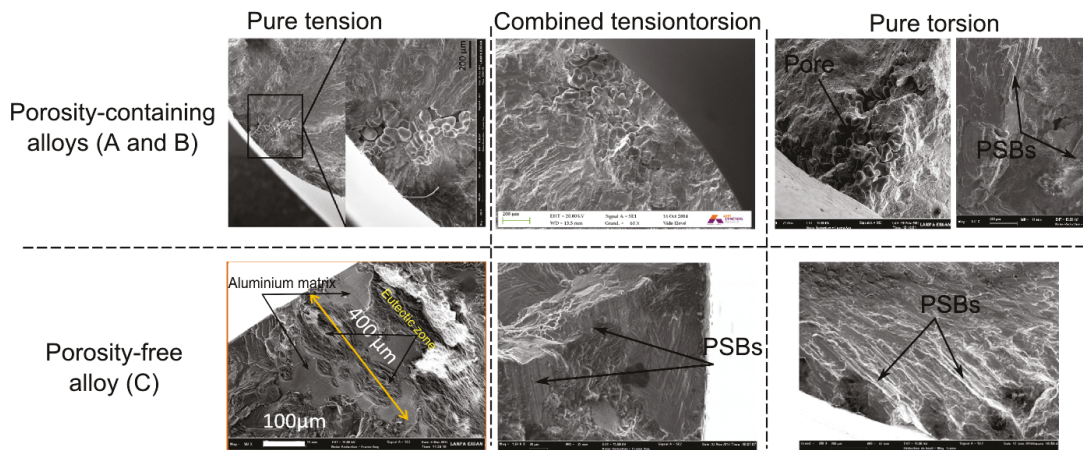


Fig. 7. Fatigue damage mechanisms of alloys A, B and C for three loading modes (pure tension, combined tension-torsion and pure torsion), observed on the fatigue failure surfaces

- For pure tension and combined tension-torsion loads: fatigue cracks always initiate and propagate from pores for the porosity-containing materials (alloys A and B) while for the porosity-free alloy (alloy C), fatigue cracks initiate from persistent slip bands (PSBs).
- For pure torsional load: for the porosity-containing alloys (alloys A and B), two crack initiation mechanisms have been observed: the first mechanism is related to crack propagation from casting pores located on the specimen surface and the second is controlled by PSB formation. These two mechanisms coexist and have been observed on the same specimen. For the porosity-free alloy (alloy C), only the crack initiation mechanism related to PSBs formation was observed.

4. Modelling framework and application to the cast alloys being investigated

4.1. The probabilistic concept for fatigue strength modelling

Initiated in the work of [7] and developed in the work of [8], the probabilistic modelling framework was initially proposed to reflect experimental observations highlighting a state of competition between two very different fatigue crack damage mechanisms in a bainitic steel [11–13]: one related to local plasticity at the mesoscopic scale and the other controlled by crack growth from clusters of MnS inclusions. In order to describe these mechanisms in a high cycle fatigue model, the authors determine the probability of failure in the material matrix Pf_1 and the probability of a crack propagating from MnS inclusion clusters Pf_2 . The weakest link concept ([14, 15]) is then used to determine the overall probability of survival of the specimen, referred to as Pf :

$$1 - Pf = (1 - Pf_1)(1 - Pf_2) \quad (1)$$

The expressions for Pf_1 and Pf_2 can be obtained via the use of any two appropriate fatigue criteria such as the Crossland-LEFM criteria combination, the Crossland-Murakami criteria combination([7]), or the Huyen [16]-LEFM criteria combination [8].

4.2. Application to cast aluminium alloys being investigated

In the section 3, it was shown that in the porosity-free alloy (alloy C), the crack initiation is principally related to persistent slip bands formation in the aluminium matrix, regardless of the loading mode. However, in the porosity-containing alloys (alloys A and B), fatigue cracks always initiate from casting porosity for both uniaxial and combined tension-torsion loads. These observations suggest that the probabilistic concept presented in the previous paragraph would be a reasonable choice to model the fatigue behaviour of the cast aluminium alloys under investigation. In this section, the choice of the criteria corresponding to each fatigue damage mechanism will be described as well as the procedure used to identify the model parameters. The predictions will be then compared with experimental fatigue strength data for the three alloys (see Tab.3).

Alloy	Pure tension (alloys B and C) Plane bending (alloy A) ($\mu \pm s$)(MPa)	Pure torsion ($\mu \pm s$)(MPa)	Combined tension-torsion $\sigma_{xx,a}(=2\tau_{xy,a})(\mu \pm s)$ (MPa)
A	82.8 ± 17.7 [10]	92.8 ± 14.1 [10]	66.1 ± 12.9
B	65.0 ± 13.3	69.0 ± 5.3	49.0 ± 10.2
C	126.1 ± 12.8	71.7 ± 7.7	80.0 ± 5.3

Table 3. Experimental values for the fatigue strength of the three alloys at 2×10^6 cycles for different multiaxial loading loads

4.2.1. Modelling of mechanism 1: crack initiation from PSB

Modelling framework.

The Dang-Van criterion ([17]) will be chosen to describe damage mechanism 1. Hence, the crack initiation condition can be defined by equation 2:

$$\sigma_{DV} \geq \sigma_{th} \quad (2)$$

where σ_{DV} is the Dang-Van equivalent stress and σ_{th} is the threshold stress. The Dang-Van equivalent stress is calculated by Eq.3:

$$\sigma_{DV} = \max_{\vec{n}}(\max_t(\tau + \alpha_{DV}\sigma_H)) \quad (3)$$

In order to take into account the scatter in the fatigue strength, a two-parameter Weibull distribution [14, 15] is used to describe the dispersion associated with the threshold stress (σ_{th}). The expression for the probability density function is :

$$f_{01}(\sigma_{th}) = \frac{m_1}{\sigma_{th0}} \left(\frac{\sigma_{th}}{\sigma_{th0}} \right)^{m_1-1} \exp\left(-\left(\frac{\sigma_{th}}{\sigma_{th0}}\right)^{m_1}\right) \quad (4)$$

where σ_{th0} is the scale parameter and m_1 is the shape parameter of the distribution. The probability of finding a grain in which a fatigue crack is initiated can be expressed as:

$$Pf_{01}(\sigma_{th} < \sigma_{DV}) = \int_0^{\sigma_{DV}} f_{01}(\sigma_{th}) d\sigma_{th} \quad (5)$$

Hence, the probability of crack initiation in an isolated grain is:

$$Pf_{01} = 1 - \exp\left(-\left(\frac{\sigma_{DV}}{\sigma_{th0}}\right)^{m_1}\right) \quad (6)$$

In order to obtain the survival probability of the entire structure, the weakest link theory [15] is used. This theory assumes that there is no interaction between crack initiation sites. Therefore, the structure can survive if, and only if, all of the grain of the considered volume can survive. Hence, the survival probability of the complete structure can be expressed by:

$$1 - Pf_1 = \prod_{M \in V_{\Omega 1}} (1 - Pf_{01}) \quad (7)$$

$$\Rightarrow Pf_1 = 1 - \exp\left(-\frac{1}{V_{\Omega 1}} \int_{V_{\Omega 1}} \left(\frac{\sigma_{DV}}{\sigma_{th0}}\right)^{m_1} dS\right) \quad (8)$$

where $V_{\Omega 1}$ represents the volume of a grain. In fact, by using the weakest link theory, size effect on the fatigue strength is taken into account. Indeed, when the considered volume being considered is increased (i.e. $V_{\Omega 1}$ is increased), the failure probability of the complete structure increases. When the stress in the volume is uniform, this expression can be simplified to:

$$Pf_1 = 1 - \exp\left(-\frac{V_{\Omega 1}}{V_{01}} \left(\frac{\sigma_{DV}}{\sigma_{th0}}\right)^{m_1}\right) \quad (9)$$

By replacing $\sigma_{th0} \left(\frac{V_{01}}{V_{\Omega 1}}\right)^{1/m_1}$ with σ'_{th0} , the probability of failure associated with damage mechanism 1 is given by:

$$Pf_1 = 1 - \exp\left(-\left(\frac{\sigma_{DV}}{\sigma'_{th0}}\right)^{m_1}\right) \quad (10)$$

Material parameter identification.

- The shape factor m_1 : this factor is determined by the following equation where $\bar{\tau}_{-1,C}$ and $\bar{\bar{\tau}}_{-1,C}$ are respectively the mean value and the standard deviation of the experimentally determined pure torsion fatigue strength (R=-1) of alloy C (i.e. porosity-free alloy):

$$\frac{\bar{\bar{\tau}}_{-1,C}}{\bar{\tau}_{-1,C}} = \frac{\sqrt{\Gamma\left(1 + \frac{2}{m_1}\right) - \Gamma^2\left(1 + \frac{1}{m_1}\right)}}{\Gamma\left(1 + \frac{1}{m_1}\right)} \quad (11)$$

$$\Rightarrow m_1 = 11.27$$

- The parameters of the Dang-Van criterion: the Dang-Van coefficient α_{DV} is determined using the following equation where $\bar{s}_{-1,C}$ is the mean value of the pure tension (R=-1) fatigue strength of alloy C:

$$\alpha_{DV} = \frac{\bar{\tau}_{-1,C} - \frac{\bar{s}_{-1,C}}{2}}{\frac{\bar{s}_{-1,C}}{3}} = 0.2049 \quad (12)$$

- The scale factor σ'_{th0} : this quantity can be determined from the experimental torsional fatigue strength data for R=-1. Its value is given by:

$$\sigma'_{th0} = \frac{\bar{\tau}_{-1,C}}{\Gamma\left(1 + \frac{1}{m_1}\right)} = 74MPa \quad (13)$$

4.2.2. Modelling of mechanism 2: fatigue damage associated with casting pores

Choice of the fatigue strength criterion.

In order to choose a suitable criterion to take into account the damage mechanism associated with casting defects, the failure surface of each tested specimen was examined to identify and measure the size of the casting defect at the origin of the fatigue failure (for alloys A and B). Fig.8 shows an example of this type of measurement.

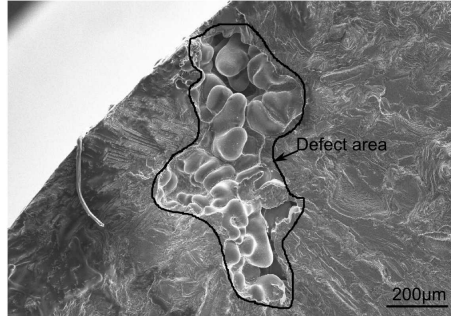


Fig. 8. Measurement of the defect size on a fatigue failure surface

Tab.4 resumes the mean value and the standard deviation of the pores at the origin of each fatigue failure. Note that for pure torsion loads ($R=-1$), because crack initiation and crack propagation are controlled by the same mechanism (i.e. controlled by the shear stress), it is very difficult to identify the crack initiation site. Therefore, the defect size reported in Tab.4 corresponds to the largest pore observed on the failure surface.

Alloy	For Uniaxial load ($\mu \pm s$)(μm)	For combined tension-torsion load ($\mu \pm s$)(μm)	For pure torsion load ($\mu \pm s$)(μm)
A	235.6 \pm 86.9	209 \pm 58.5	220 \pm 60
B	709.9 \pm 332	669 \pm 457	690 \pm 400
C	No pores found	No pores found	No pores found

Table 4. Defect sizes observed on rupture surface

Fig.9 shows the Kitagawa-Takahashi diagram of the three alloys: alloys A, B and a third data set corresponding to fatigue test conducted on specimens with the same chemical composition and heat treatment as Alloy A, but the material was gravity-sand cast in the form of bars ([18]). This alloy has approximately the same SDAS as alloy A but the casting defects size is much higher. Note that the vertical error bars corresponds to 10% to 90% probability of failure and the horizon error bars indicate 10% to 90% probability of occurrence of a defect size initiating the fatigue failure. For the third data set (Bellett et al. [18]), because the fatigue strength at $2 \cdot 10^6$ cycles was estimated from a Wöhler curve, the error bar for the fatigue strength is not reported. The experimental data are compared to the fatigue strength predictions using the LEFM criterion in which the fatigue strength is determined by the following expression:

$$2 \cdot \sigma_{1,a} = \frac{\Delta K_{th}}{0.65 \sqrt{\pi \sqrt{area}}} \quad (14)$$

where $\sigma_{1,a}$ is the amplitude of the principal stress and ΔK_{th} is the stress intensity threshold range for tension-compression loads ($R=-1$). The stress intensity thresholds have been arbitrarily estimated to match the experimental data.

Firstly, this figure shows that the slope matching the experimental data of alloy A and the alloy investigated in the work of Bellett et al. (which has the same microstructure, chemical composition and SDAS) is approximately equal to 1/2. With regard to the difference between the mean values of the fatigue strength

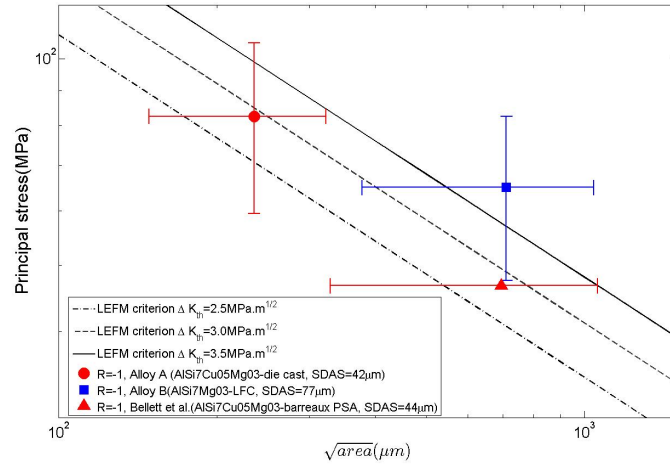


Fig. 9. A Kitagawa-Takahashi type diagram for alloys A, B and a third data set corresponding to fatigue tests conducted on specimens with the same chemical composition and heat treatment as Alloy A, but the material was gravity-sand cast in the form of bars ([18]) for pure tension load ($R=-1$), compared to the predictions using the LEFM criterion

of the Bellett et al alloy and alloy B, while these two alloys have the same casting defect size, it must be kept in mind that there are two differences between these two alloys: (1) the chemical composition (the alloy investigated in the work of Bellett et al. (AlSi7Cu05Mg03) contains $0.5\text{wt.}\%$ copper while alloy B (AlSi7Mg03) does not and (2) the SDAS ($77.6 \pm 18.9\mu\text{m}$ for alloy B and $43.8 \pm 10.8\mu\text{m}$ for the alloy studied by Bellett et al.).

It can be seen that the values of the estimated SIF threshold for a load ratio of $R=-1$ for alloy A is approximately $2.5 \text{ MPa} \sqrt{\text{m}}$. This value is low compared to the artificial long crack growth threshold reported in the literature, even though only experimental data for a load ratio of $R=0.1$ has been found ($\Delta K_{th,lc,R=0.1} \approx 3.5$ to $5.5 \text{ MPa} \sqrt{\text{m}}$, [19–23]). This suggests that the small crack effect is significant for natural fatigue crack growth in the threshold regime.

To investigate the small crack effect on natural fatigue crack growth, a comparison between the crack growth rate of a natural fatigue crack (observed on the specimen surface during a fatigue test) and the artificial long crack growth rate (determined by a crack propagation test using a Single Edge Notched specimen) is presented in Fig.10. The SIF of the natural fatigue crack is determined by using equation 15([9]) and by assuming that the crack shape can be approximated by two equilateral triangles of side length, a , (i.e. the demi-crack length on the surface).

$$\Delta K = 2\sigma_a \times 0.65 \times \sqrt{\pi \sqrt{areal}} \quad (15)$$

It is shown that the natural fatigue crack growth rates are much higher for the artificial long crack at the same load ratio $R=-1$. This is particularly true in the threshold crack growth domain ($d(2a)/dN < 10^{-8} \text{ m/cycle}$). This small crack effect associated with natural fatigue cracks was also observed in the work of Roy et al. [24]. Regarding the crack growth threshold, although not enough experimental data has been obtained to accurately determine the exact value of the SIF threshold for natural crack growth, it can be seen that, at a growth rate of $d(2a)/dN = 10^{-9} \text{ m/cycle}$, the threshold of natural fatigue cracks is much lower than that of artificial long cracks. This is in agreement with the SIF threshold of alloy A determined using LEFM criterion (see Fig.9)

From this point of view, the LEFM criterion will be chosen to describe the second crack initiation mechanism.

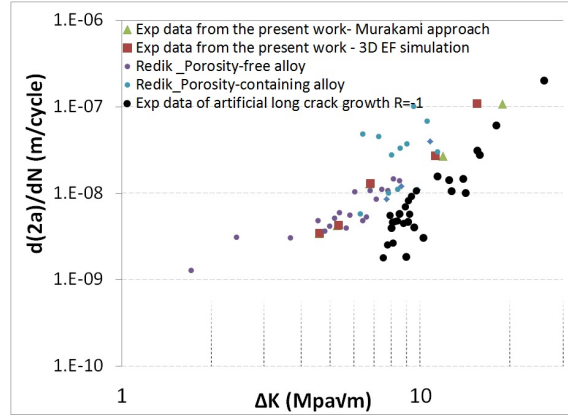


Fig. 10. Comparison of crack growth rate between natural fatigue cracks and artificial long cracks (black points)

Modelling framework.

For this damage mechanism it will be assumed that cracks are very easily initiated at casting defects. Hence, the fatigue strength is determined by the "non-propagation" of these cracks. Based on linear elastic fracture mechanics (LEFM), a crack will propagate from a pore if the following condition is satisfied:

$$\Delta K \geq \Delta K_{th} \quad (16)$$

Where ΔK_{th} is the SIF threshold. By analogy with the first mechanism (see Eq.4), the Weibull distribution will be used to describe the scatter associated with the stress intensity threshold:

$$f_{02}(\Delta K_{th}) = \frac{m_2}{\Delta K_{th0}} \left(\frac{\Delta K_{th}}{\Delta K_{th0}} \right)^{m_2-1} \exp \left[- \left(\frac{\Delta K_{th}}{\Delta K_{th0}} \right)^{m_2} \right] \quad (17)$$

Where m_2 is the shape parameter and ΔK_{th0} is the scale factor.

Hence, the probability of crack growth from an isolated pore can be expressed by:

$$P f_{02} = 1 - \exp \left(- \left(\frac{\Delta K}{\Delta K_{th0}} \right)^{m_2} \right) \quad (18)$$

For a uniform macroscopic stress distribution, this expression becomes:

$$P f_2 = 1 - \exp \left(- \frac{V_{\Omega 2}}{V_{02}} \left(\frac{\Delta K}{\Delta K_{th0}} \right)^{m_2} \right) \quad (19)$$

Where $V_{\Omega 2}$ is the total loaded volume and V_{02} represents the volume associated with a crack emanating from an isolated pore. By making the following substitution $\Delta K'_{th0} = \Delta K_{th0} \left(\frac{V_{02}}{V_{\Omega 2}} \right)^{1/m_2}$ the volume effect is neglected and the failure probability associated with damage mechanism 2 for the complete structure is given by:

$$P f_2 = 1 - \exp \left(- \left(\frac{\Delta K}{\Delta K'_{th0}} \right)^{m_2} \right) \quad (20)$$

Material parameter identification.

- The shape factor m_2 : this factor can be identified by the following equation:

$$\frac{\bar{s}_{-1,A/B}}{\bar{s}_{-1,A/B}} = \frac{\sqrt{\Gamma \left(1 + \frac{2}{m_2} \right) - \Gamma^2 \left(1 + \frac{1}{m_2} \right)}}{\Gamma \left(1 + \frac{1}{m_2} \right)} \quad (21)$$

where $\bar{s}_{-1,A/B}$ and $\bar{s}_{-1,A/B}$ are the standard deviation and the mean value respectively of the tension-compression fatigue strength (R=-1) for alloys A or B. A value of $m_2 = 5.37$ for alloy A and $m_2 = 5.59$ for alloy B is obtained.

- The scale factor $\Delta K'_{th0}$: this factor can be determined using the mean value of the fully reserved tension-compression fatigue strength, \bar{s}_{-1} , of alloy A or B by the following equation:

$$2\bar{s}_{-1,B} \times 0.65 \sqrt{\pi \sqrt{area}} = \Delta K'_{th0} \Gamma \left(1 + \frac{1}{m_2} \right) \quad (22)$$

A value of value of $\Delta K'_{th0} = 3.2 MPa \sqrt{m}$ is obtained for alloy A and $\Delta K'_{th0} = 4.3 MPa \sqrt{m}$ for alloy B.

4.2.3. Methodology to take into account both fatigue damage mechanisms

As mentioned earlier, failure of the complete structure is caused by the "dominant" fatigue damage mechanism. Hence, the "total" survival probability is the result of a competition between the two coexisting damage mechanisms. If the mechanisms are assumed to be independent, the weakest link theory can be used to determined the total probability of failure via the following equation:

$$1 - Pf = (1 - Pf_1)(1 - Pf_2) \quad (23)$$

4.3. Results and discussions

The results of the modelling approach described above are presented in Fig.11 for different loading modes.

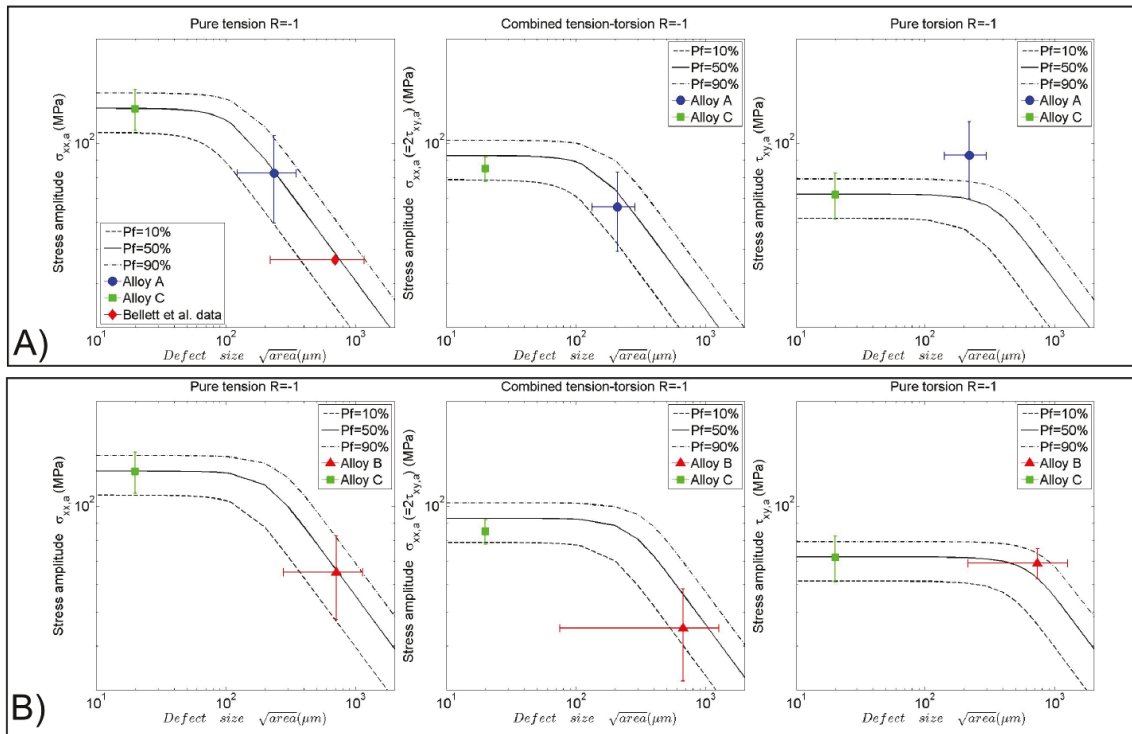


Fig. 11. Correlation between the experimental data and the model predictions: A) the experimental data for alloys C and A are used to identify the material parameters of the first and the second mechanisms respectively; B) the experimental data for alloys C and B are used to identify the material parameters of the first and the second mechanisms respectively.

It is important to note that the modelling framework presented above leads naturally to Kitagawa-Takahashi type diagrams, which are multiaxial and probabilistic.

Concerning the correlation between the experimental data and model predictions, following conclusions could be made:

- For tension-compression loads: the model predictions are well match with the experimental data. However, note that the experimentally determined tension-compression fatigue strength of alloys A or B and C were used to identify the model parameters.
- For combined tension-torsion loads: slightly non-conservative predictions are observed.
- For pure torsional loads: a large difference between the experimental data and the model predictions for alloy A is observed. As discussed in Section.3 observations on the specimen surface as well as SEM inspection of the failure surfaces for pure torsional loads show that the role of casting pores is secondary, compared to the formation of PSBs. In other words, the role of the aluminium matrix, which is related to the DAS/SDAS and the hardening level, is dominant. From this point of view, the difference can be explained by the following factors:
 - Alloy A contains an additional 0.5%wt. copper compared to alloys B and C. The presence of Cu in the chemical composition results in higher micro-hardness of the alpha phase. This causes the critical shear stress for PSB formation to be higher for alloy A compared to alloys B and C. Consequently, the macroscopic pure torsional fatigue strength of alloy A is higher. However, the torsion fatigue strength of alloy C was used to identify the model parameters related to the Dang-Van criterion and mechanism 1 (see Eq.12). In order to improve the model, torsional fatigue tests would need to be conducted on an alloy with the same microstructure (i.e. DAS/SDAS and micro-hardness) as alloy A but without casting defects (using the HIP treatment for example). Never-the-less, it should be kept in mind that the macroscopic pure torsional fatigue strength is also influenced by the DAS/SDAS via the grain boundary effect on the stress field at the mesoscopic scale. This effect is not studied in the present work.
 - It can be seen that the model can predict a critical defect size of $\sqrt{area} \approx 400$ to $600\mu\text{m}$ for the pure torsional load. This prediction is in good agreement with experimental observations of the failure surfaces. Compared to the critical defect size for tension-compression loads of $\sqrt{area} \approx 100$ to $200\mu\text{m}$, a lower influence of casting defects on the pure torsional fatigue strength can be confirmed.
- It is shown that the crack growth thresholds of alloys A and B are different (see Eq.22). These two materials differ principally in terms of their SDAS. A modelling approach including the influence of the SDAS will be introduced in a future publication.

5. Conclusions

The principal conclusions of this work can be summarised as follows:

- The characterisation of the HCF damage mechanisms operating in the three cast aluminium alloys indicate that:
 - For tension-compression ($R=-1$) and combined tension-torsion ($R=-1$, $k = \tau_a/\sigma_a = 0.5$) loads, fatigue cracks initiate from pores, for the porosity-containing alloys (alloys A and B) while for the porosity-free alloy (alloy C), fatigue cracks initiate principally from PSBs.
 - For pure torsion loads ($R=-1$), only the first damage mechanism related to PSBs was observed for alloy C. For the porosity-containing alloys (alloys A and B), two damage mechanisms have been observed: the first mechanism is controlled by PSB formation and the second is related to crack propagation from porosity located on the specimen surface.

- The short crack effect was observed for natural fatigue crack propagation.
- Casting pores have less influence for pure torsional loads when compared to the other two loading conditions studied. Or, stated in a different way, the critical defect size is much higher in torsion compared to the other loading modes.
- Regarding the proposed probabilistic modelling framework and the criteria choices, it can be concluded that:
 - The model leads naturally to probabilistic, multiaxial Kitagawa-Takahashi type diagrams, which can be used to explain the relationship between the fatigue behaviour of the material and the different casting processes and post-casting heat treatments (via the porosity size distribution). Another advantage of this approach is its flexibility. Any two fatigue criteria can be used in the framework. They just need to be suitable for modelling the two damage mechanisms.
 - The results issued from the DangVan-LEFM criteria combination are very encouraging for the cast aluminium alloys under investigation, especially given the factors discussed in Section 4.3 above.

Acknowledgement

This work was financially supported by PSA Peugeot Citroën.

References

- [1] K. S. Chan, P. Jones, Q. Wang, Fatigue crack growth and fracture paths in sand cast {B319} and {A356} aluminum alloys, *Materials Science and Engineering: A* 341 (12) (2003) 18 – 34. doi:[http://dx.doi.org/10.1016/S0921-5093\(02\)00196-X](http://dx.doi.org/10.1016/S0921-5093(02)00196-X). URL <http://www.sciencedirect.com/science/article/pii/S092150930200196X>
- [2] M. S. A. T. S. R. KS, M. KSS, Fatigue properties of sand cast, stircast and extruded Al7Si03Mg alloy with trace additions of Bi and Mn, *Materials transactions, JIM* 38 (1) (1997) 28–36.
- [3] D. McDowell, K. Gall, M. Horstemeyer, J. Fan, Microstructure-based fatigue modeling of cast Al356-T6 alloy, *Engineering Fracture Mechanics* 70 (1) (2003) 49 – 80. doi:[http://dx.doi.org/10.1016/S0013-7944\(02\)00021-8](http://dx.doi.org/10.1016/S0013-7944(02)00021-8). URL <http://www.sciencedirect.com/science/article/pii/S0013794402000218>
- [4] S.-h. C. Gordon W. Powell, Carroll E. Mobley, *A fractography atlas of casting alloys*, Battelle Press, 1992.
- [5] I. Koutiri, Effet des fortes contraintes hydrostatiques sur la tenue en fatigue des matériaux métalliques, Ph.D. thesis, ENSAM (2011).
- [6] J.-Y. Buffière, S. Savelli, P. Jouneau, E. Maire, R. Fougères, Experimental study of porosity and its relation to fatigue mechanisms of model AlSi7Mg0.3 cast alloy, *Materials Science and Engineering: A* 316 (12) (2001) 115 – 126. doi:[http://dx.doi.org/10.1016/S0921-5093\(01\)01225-4](http://dx.doi.org/10.1016/S0921-5093(01)01225-4). URL <http://www.sciencedirect.com/science/article/pii/S0921509301012254>
- [7] E. Pessard, D. Bellett, F. Morel, I. Koutiri, A mechanistic approach to the Kitagawa-Takahashi diagram using a multiaxial probabilistic framework, *Engineering Fracture Mechanics* (0) (2013) –. doi:<http://dx.doi.org/10.1016/j.engfracmech.2013.06.001>. URL <http://www.sciencedirect.com/science/article/pii/S001379441300218X>
- [8] I. Koutiri, D. Bellett, F. Morel, E. Pessard, A probabilistic model for the high cycle fatigue behaviour of cast aluminium alloys subject to complex loads, *International Journal of Fatigue* 47 (0) (2013) 137 – 147. doi:<http://dx.doi.org/10.1016/j.ijfatigue.2012.08.004>. URL <http://www.sciencedirect.com/science/article/pii/S0142112312002472>
- [9] Y. Murakami, *Effects of small defects and nonmetallic inclusions*, Elsevier, 2002.
- [10] I. Koutiri, D. Bellett, F. Morel, L. Augustins, J. Adrien, High cycle fatigue damage mechanisms in cast aluminium subject to complex loads, *International Journal of Fatigue* 47 (0) (2013) 44 – 57. doi:<http://dx.doi.org/10.1016/j.ijfatigue.2012.07.008>. URL <http://www.sciencedirect.com/science/article/pii/S0142112312002356>
- [11] E. Pessard, F. Morel, A. Morel, The anisotropic fatigue behavior of forged steel, *Advanced Engineering Materials* 11 (9) (2009) 732–735. doi:10.1002/adem.200900040. URL <http://dx.doi.org/10.1002/adem.200900040>
- [12] E. Pessard, F. Morel, A. Morel, D. Bellett, Modelling the role of non-metallic inclusions on the anisotropic fatigue behaviour of forged steel, *International Journal of Fatigue* 33 (4) (2011) 568 – 577. doi:<http://dx.doi.org/10.1016/j.ijfatigue.2010.10.012>. URL <http://www.sciencedirect.com/science/article/pii/S0142112310002471>

- [13] E. Pessard, F. Morel, C. Verdu, L. Flacelire, G. Baudry, Microstructural heterogeneities and fatigue anisotropy of forged steels, *Materials Science and Engineering: A* 529 (0) (2011) 289 – 299. doi:<http://dx.doi.org/10.1016/j.msea.2011.09.031>. URL <http://www.sciencedirect.com/science/article/pii/S0921509311009919>
- [14] W. Weibull, *A Statistical Theory of the Strength of Materials*, Generalstabens litografiska anstalts frlag, 1939.
- [15] W. Weibull, A statistical distribution function of wide applicability, *Journal of Applied Mechanics* 18 (1951) 293–297.
- [16] T. T. H. Nguyen, Effet des hétérogénéités microstructurales sur le comportement en fatigue multiaxiale a grand nombre de cycles, Ph.D. thesis, Arts et Metiers ParisTech, Centre d'Angers LPMI (2008).
- [17] DangVan, Sur la resistance a la fatigue des metaux, *Sciences et techniques de l'armement* (47) (1973) 641–772.
- [18] D. Bellett, F. Morel, Influence des fortes contraintes hydrostatiques sur la resistance en fatigue dun alliage daluminium as7g03u, Tech. rep., SERAM Centre d'Angers (2005).
- [19] M. Caton, J. Jones, J. Allison, The influence of heat treatment and solidification time on the behavior of small-fatigue-cracks in a cast aluminum alloy, *Materials Science and Engineering: A* 314 (12) (2001) 81 – 85. doi:[http://dx.doi.org/10.1016/S0921-5093\(00\)01916-X](http://dx.doi.org/10.1016/S0921-5093(00)01916-X). URL <http://www.sciencedirect.com/science/article/pii/S092150930001916X>
- [20] M.J.Caton, J.W.Jones, H.Mayer, S. Stanzl-Tschegg, J.E.Allison, Demonstration of an endurance limit in cast 319 aluminum, *Metallurgical and Materials Transactions A* 34 (11) (2003) 33–41.
- [21] E. Merhy, Propagation de fissure sous chargement thermomécanique cyclique anisotherme: Application au dimensionnement de structures automobiles en alliage d'aluminium (al-si), Ph.D. thesis, Ecole Polytechnique de Paris (2011).
- [22] B. Skallerud, T. Iveland, G. Hrkegrd, Fatigue life assessment of aluminum alloys with casting defects, *Engineering Fracture Mechanics* 44 (6) (1993) 857 – 874. doi:[http://dx.doi.org/10.1016/0013-7944\(93\)90108-5](http://dx.doi.org/10.1016/0013-7944(93)90108-5). URL <http://www.sciencedirect.com/science/article/pii/0013794493901085>
- [23] T. Mbuya, I. Sinclair, A. Moffat, P. Reed, Micromechanisms of fatigue crack growth in cast aluminium piston alloys, *International Journal of Fatigue* 42 (0) (2012) 227 – 237, *fatigue Damage of Structural Materials {VIII}*. doi:<http://dx.doi.org/10.1016/j.ijfatigue.2011.10.015>. URL <http://www.sciencedirect.com/science/article/pii/S0142112311002921>
- [24] M. Roy, Y. Nadot, C. Nadot-Martin, P-G. Bardin, D. Maijer, Multiaxial kitagawa analysis of a356-t6, *International Journal of Fatigue* 33 (6) (2011) 823 – 832. doi:<http://dx.doi.org/10.1016/j.ijfatigue.2010.12.011>. URL <http://www.sciencedirect.com/science/article/pii/S0142112310003129>